Chinese Journal of Mechanical Engineering

ORIGINAL ARTICLE

Open Access

Design and Simulation of Flow Field for Bone Tissue Engineering Scaffold Based on Triply Periodic Minimal Surface

Zhen Wang[1], Chuanzhen Huang[1*], Jun Wang[2], Peng Wang[1], Shisheng Bi[1] and Ch Asad Abbas[1]

Abstract

A novel method was proposed to design the structure of a bone tissue engineering scaffold based on triply periodic minimal surface. In this method, reverse engineering software was used to reconstruct the surface from point cloud data. This method overcomes the limitations of commercially available software packages that prevent them from generating models with complex surfaces used for bone tissue engineering scaffolds. Additionally, the fluid field of the scaffolds was simulated through a numerical method based on finite volume and the cell proliferation performance was evaluated via an in vitro experiment. The cell proliferation and the mass flow evaluated in a bioreactor further verified the flow field simulated using computational fluid dynamics. The result of this study illustrates that the pressure value drops rapidly from 0.103 Pa to 0.011 Pa in the *y*-axis direction and the mass flow is unevenly distributed in the outlets. The mass flow in the side outlets is observed to be approximately 24.3 times higher than that in the bottom outlets in the range 6.13×10^{-8} kg/s to 1.49×10^{-6} kg/s. Moreover, the mass flow in the bottom outlets decreases from the center to the edge, whereas the mass flow in the side outlets decreases from the top to the bottom. Importantly, although the mean value of wall shear stress is significantly more than 0.05 Pa, there is still a large area with a suitable shear stress below 0.05 Pa where most cells can proliferate well. The result shows that the inlet velocity 0.0075 m/s is suitable for cell proliferation in the scaffold. This study provides an insight into the design, analysis, and in vitro experiment of a bone tissue engineering scaffold.

Keywords: Bone tissue engineering, Porous scaffold, Flow field, Reverse engineering, Cell proliferation

1 Introduction

According to recent studies [1, 2], millions of people are suffering severely from orthopedic disorders caused by traffic accidents, bone tumors, infection, etc. Bone can heal by itself when a small segment defect occurs; however, despite recent advances in medical technologies, treatment of a non-healable size bone defect is still challenging. Tissue engineering, which is a promising method for the reconstruction of bone, is an interdisciplinary field that applies the principles of engineering and life sciences toward the development of biological substitutes for restoring, maintaining, or improving tissue function [3]. It has been applied to the construction of some tissues and organs such as bone, cartilage, skin, and liver [4, 5]. Cell, scaffold, and growth factor are the three most important conditions in tissue engineering. Some ideal properties are required for the bone scaffold [6–10].

The porous scaffold should have appropriate pore size, morphology, and porosity for cell adhesion, migration, proliferation, and differentiation. The materials of the scaffold should have osteoinduction and good biocompatibility. Moreover, controllable biodegradability is a desired property for a bone tissue engineering scaffold, which should have a suitable degradation rate corresponding to the cell growth rate. The scaffold should also have sufficient mechanical strength to support human body, and appropriate elasticity modulus to match that of bone.

*Correspondence: huangcz@sdu.edu.cn
[1] Centre for Advanced Jet Engineering Technologies (CaJET), Key Laboratory of High-efficiency and Clean Mechanical Manufacture (Ministry of Education), School of Mechanical Engineering, Shandong University, Jinan 250061, China
Full list of author information is available at the end of the article

Numerous modeling methods have been proposed to design the structure of a bone scaffold, among which computer-aided design (CAD)-based modeling is the most common method. Currently, most commercial CAD tools are based on solid modeling systems, such as constructive solid geometry. For this modeling method, complex models are designed and represented by combining standard solid primitives (cylinders, spheres, or cubes). It is only possible to create regular solids without complex surfaces through this process. However, with the rapid development of 3D printing technology in tissue engineering, more complex shaped models can be processed; hence, a new modeling method to design a scaffold structure considering a complex environment for cell growth and for supporting human body is urgently required.

Triply periodic minimal surface (TPMS) can describe several natural shapes—for example, cubosomes and certain cell membranes or prolamellar bodies of plants [11–14]. In the bio-manufacturing field, TPMS allows the design of scaffolds with very high surface-to-area ratios, enhancing cell proliferation. Melchels et al. [15, 16] presented a scaffold design methodology by using K3DSurf v.0.6.2 software and generated TPMS models that describe gyroid architectures. However, there are few reports about other methods to construct a bone tissue engineering scaffold based on TPMS, and the fluid field distribution in the TPMS scaffold is still not clear. In this paper, a novel method with a high degree of design freedom to obtain smooth surfaces is proposed to construct TPMS scaffold models applicable to bone tissue engineering. In addition, the flow field in the scaffold is analyzed through a numerical simulation method. This study provides an insight into the design of a bone tissue engineering scaffold and the analysis of cell proliferation performance based on the flow field.

2 Materials and Methods

2.1 Building of TPMS Scaffold Models

A TPMS scaffold was obtained via the following three steps: calculation of point cloud data, reconstruction of a surface model, and generation of a solid model.

The concept of minimal surface was first proposed by Lagrange [17] in 1760 to determine the surface with the smallest area for a constant perimeter. Subsequently, in 1785, Meusnier [18] proved that the mean curvature (H) at any point on the surface is zero. The mean curvature of the surface can be described by Eq. (1):

$$H = \frac{k_1 + k_2}{2}, \tag{1}$$

where k_1 and k_2 are the principle curvatures of the surface at that point.

Schnering and Nesper [19] used the implicit function given in Eq. (2) to describe a Schwarz primitive surface mathematically, which was a typical example of TPMS:

$$\cos x + \cos y + \cos z = 0, \tag{2}$$

where $x \in [-3.14, 3.14]$, $y \in [-3.14, 3.14]$, and $z \in [-3.14, 3.14]$.

MATLAB is a commercial mathematical computing software program that can perform matrix operations, draw functions, and implement algorithms, and is mainly used in engineering computing, signal processing, image processing, and some other applications. This software program was utilized to compute the point cloud data using Eq. (2).

Subsequently, the point cloud data were sent to a reverse engineering software program (Geomagic Studio) to complete the surface reconstruction. The coordinates of the points, such as (3.14, 1.57, 0), were calculated using MATLAB without units. Thus, the unit millimeter was selected and a scale factor of 0.1 was simultaneously implemented on all the coordinates. For example, the coordinates mentioned above became (0.314 mm, 0.157 mm, 0 mm) after the transformation.

As shown in Figure 1, the TPMS surface models were reconstructed from 560 points/mm^2, 1120 points/mm^2 and 5600 points/mm^2. It was observed that 5600 points/mm^2 were sufficient to obtain a smooth surface. Therefore, in the following steps, all the surface models were reconstructed from 5600 points/mm^2.

The surface model was thickened by 0.1 μm, 20 μm, 40 μm, and 60 μm in CAD software (SolidWorks) to form different pore diameters 314 μm, 354 μm, 394 μm, and 434 μm, respectively. In previous studies, most researchers selected a pore diameter ranging from 300–900 μm in bone tissue engineering, which showed effective results for bone reconstruction [20–22]. Subsequently, the surface model was transformed to a solid model through Boolean operation with a cube (628 μm × 628 μm × 628 μm), which could be expanded to a 27-unit scaffold via an array operation as shown in Figure 2.

2.2 Simulation of Flow Field

The cell culture medium was assumed to be a homogeneous, viscous, and incompressible Newtonian fluid; therefore, the differential equations of motion (Navier–Stokes equation) can be described by Eq. (3):

$$\begin{cases} \frac{\mathrm{d}v_x}{\mathrm{d}t} = f_x - \frac{1}{\rho}\frac{\partial p}{\partial x} + \nu \cdot \nabla^2 v_x, \\ \frac{\mathrm{d}v_y}{\mathrm{d}t} = f_y - \frac{1}{\rho}\frac{\partial p}{\partial y} + \nu \cdot \nabla^2 v_y, \\ \frac{\mathrm{d}v_z}{\mathrm{d}t} = f_z - \frac{1}{\rho}\frac{\partial p}{\partial z} + \nu \cdot \nabla^2 v_z, \end{cases} \tag{3}$$

where v_x, v_y, and v_z are the velocity components in the directions of x-, y-, and z-axes, respectively; f_x, f_y, and

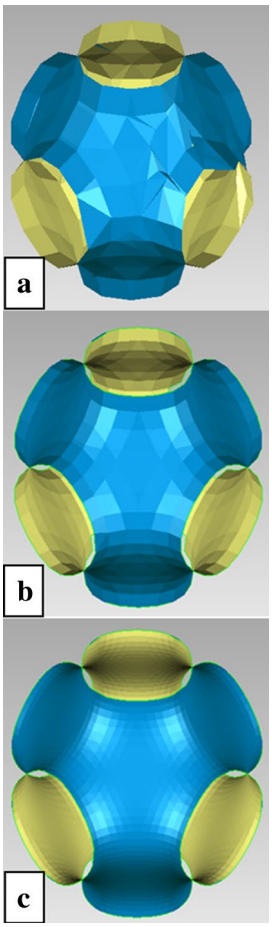

Figure 1 Surface models of bone scaffolds: **a** 560 points/mm^2, **b** 1120 points/mm^2, **c** 5600 points/mm^2

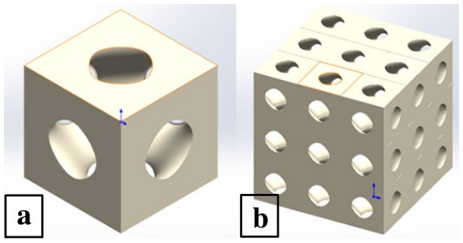

Figure 2 Solid models of bone scaffolds: **a** single-unit model, **b** 27-unit model

f_z are force components in the directions of x-, y-, and z-axes, respectively; ρ is the fluid density; v is the fluid kinematic viscosity; p is the fluid pressure; ∇ is the differential operator.

The computational fluid dynamics (CFD) model must be meshed before obtaining the final solution through CFD software (ANSYS). To obtain a more accurate result, an inflation meshing method was applied to the model boundary as shown in Figure 3, where the maximum number of layers was set as 5 and the growth rate was set as 1.25.

The top nine pores were set as the velocity inlet (0.01 m/s, 0.0075 m/s, 0.005 m/s, 0.0025 m/s), whereas the other 45 pores were set as the pressure outlet (0 Pa); furthermore, the material was set as the cell culture medium with two preset parameters (density is 1000 kg/m^3, viscosity is 0.0018 Pa·s) obtained from Ref. [23].

The finite volume method was used to evaluate and simulate the flow field of the bone tissue engineering scaffold via a quantitative investigation of the relationship between the pore diameters and wall shear stress, as well as the inlet velocity and mass flow.

2.3 Cell Culture

The scaffolds were manufactured via 3D printing with a type of biodegradable organic polymer material, as shown in Figure 4. Based on the machining accuracy, the scaffolds with the pore diameters of 314 μm and 434 μm were selected as experimental samples. Subsequently, the pore size of the samples was measured using a Keyence Laser Microscope and the porosity was measured using a Sartorius Porosimeter. Before performing cell culture experiments with the scaffold samples, to achieve thorough sterilization, the samples were immersed in 90% alcohol for 10 h and exposed to a UV lamp for 2 h.

Bone marrow mesenchymal stem cells (BMSCs) were cultured in the scaffolds placed in a perfusion bioreactor, and the cell proliferation performance was evaluated to verify the CFD simulation result. First, BMSCs were extracted from the femur of a four-week-aged Wistar rat, provided by Shandong University Laboratory Animal Center. Subsequently, the BMSCs were primarily cultured with 90% Dulbecco's modified eagle medium, 10% fetal bovine serum, and 100 U/mL penicillin-streptomycin. The cell culture medium was replaced after 24 h, and subsequently, it was replaced every 48 h. After 7 days of primary culture, when the BMSCs were spread over the bottom of the culture dish, they were digested down using 0.25% trypsin-ethylenediaminetetraacetic acid solution. The cell suspension was adjusted to one million cells per milliliter using the cell counting chamber under the optical microscope. Subsequently, the cell suspension was seeded on the scaffolds settled in a perfusion bioreactor developed by our research group as shown in Figure 5, which could monitor the velocity and mass flow of the inlets and outlets. Subsequently, the perfusion bioreactor was placed in a CO_2 cell incubator under the conditions of 37 °C, 5% CO_2, and 80% relative humidity. The cell culture medium was replaced every 48 h.

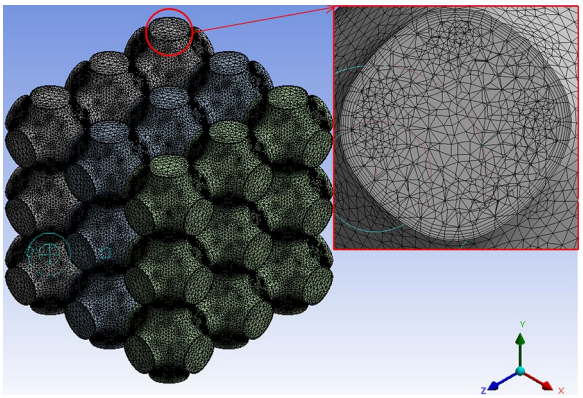

Figure 3 Mesh models of bone scaffolds in the CFD software

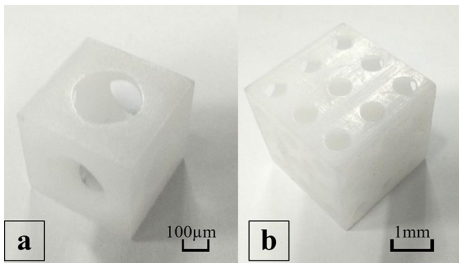

Figure 4 Bone scaffolds: **a** single-unit model, **b** 27-unit model

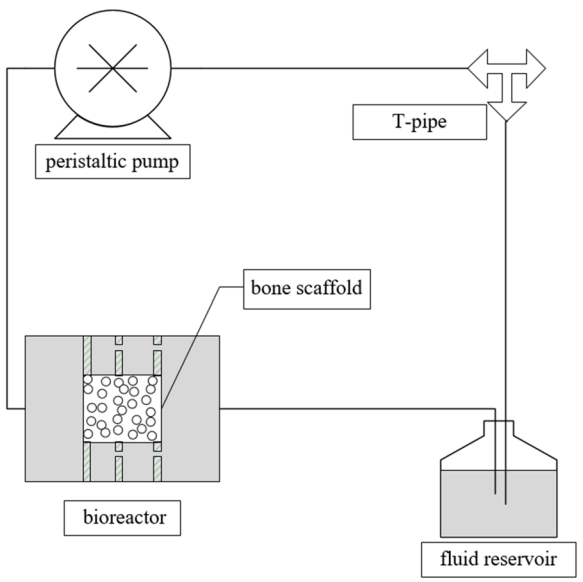

Figure 5 Schematic diagram of the perfusion bioreactor

A methyl thiazol tetrazolium (MTT) assay, which could be reduced by active cells into insoluble purple formazan granules, was used to test cell proliferation in the scaffold on days 1, 4, 7, and 10. Specifically, after the MTT solution was added to each sample, the sample was required to be incubated in a cell incubator under the conditions of 37 °C, 5% CO_2, and 80% relative humidity for 4 h. Subsequently, the medium was removed and the sample was immersed in dimethyl sulfoxide, which could dissolve the precipitated formazan. Finally, the absorbance value was observed using a UV–vis spectrophotometer at 570 nm.

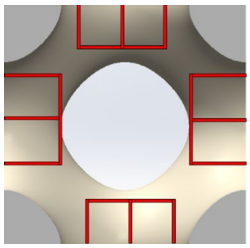

Figure 6 Eight observation areas on the surface of the bone scaffold

On the 10th day, the scaffold sample was cut into two symmetrical parts. Figure 6 shows eight similar areas (100 μm × 100 μm) on the surface of the scaffold observed using a fluorescence microscope. In addition, eight microscope pictures were assembled together to form a global picture for a comparison with the CFD simulation results to confirm our conclusion.

Figure 7 shows the general flowchart of this study.

3 Results and Discussion

3.1 Geometry Details

Four TPMS scaffold models with different pore diameters were obtained by using different scale factors and thickening factors. These scaffold models had porosities ranging from 51.7% to 68.8% and various wall areas ranging from 7.865×10^{-7} m^2 to 8.923×10^{-7} m^2. As the 27-unit model was obtained from the single-unit model via an array operation, the single-unit model could be used to represent the 27-unit model to a certain extent. The geometry details of the single-unit model are presented in Table 1.

The porosity increased with the increase in the pore diameter and simultaneously the wall area shrank rapidly as shown in Table 1. Generally, with regard to the porous scaffolds, higher porosity indicates lower strength and lower elastic modulus [24, 25]. However, higher porosity can promote the transportation of oxygen and nutrients and improve the metabolism system. Therefore, it is still a significant challenge to balance the mechanical and biological properties.

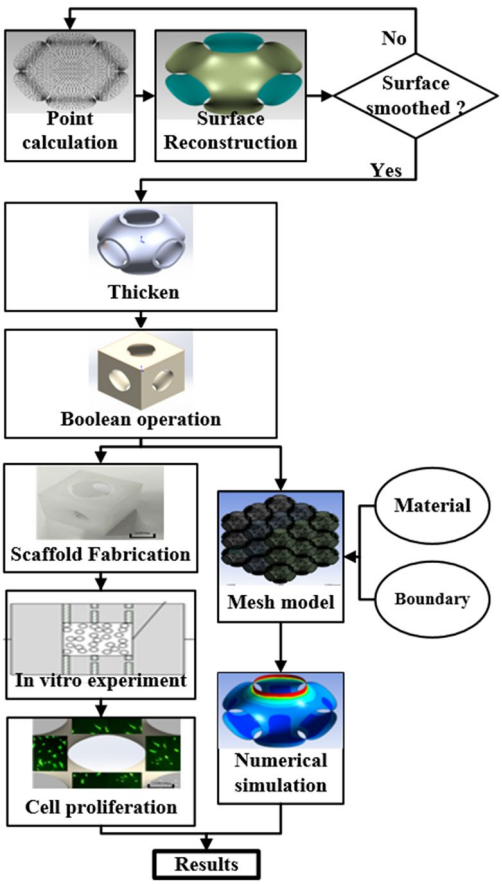

Figure 7 General flowchart of this study

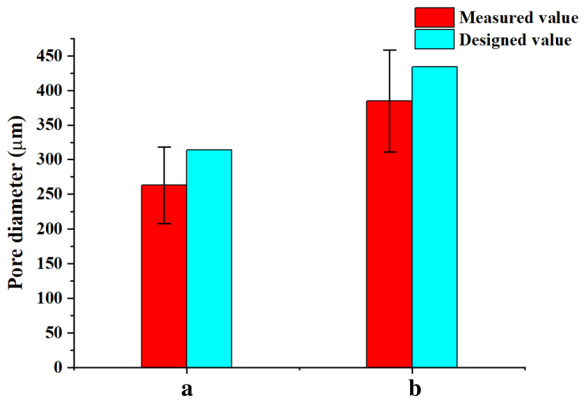

Figure 8 Pore diameter: **a** designed value 314 μm, **b** designed value 434 μm

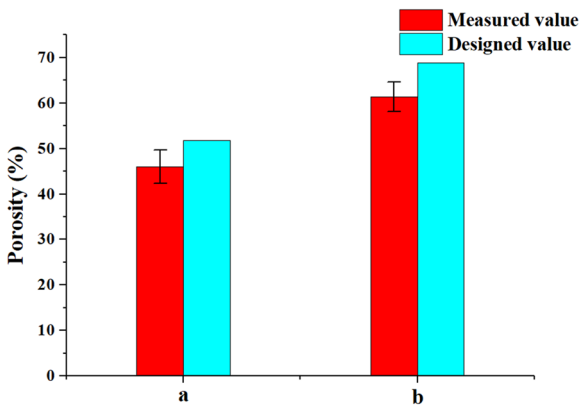

Figure 9 Porosity: **a** designed value 51.7%, **b** designed value 68.8%

Table 1 Geometry details of the single-unit model

Pore diameter (μm)	Porosity (%)	Wall area (m^2)
314	51.7	8.923×10^{-7}
354	55.4	8.861×10^{-7}
394	61.9	8.367×10^{-7}
434	68.8	7.865×10^{-7}

Five samples identical in all dimensions were fabricated to obtain reliable results. However, only the scaffolds with the pore diameters of 314 μm and 434 μm were selected as the experimental samples, because of the poor machining accuracy. Figure 8 and Figure 9 indicate that the measured values of pore diameter and porosity are slightly lower than the designed values for the samples with the pore diameters of 314 μm and 434 μm, which therefore influenced the verification of the results of CFD simulation and cell proliferation to a certain degree.

3.2 Flow Field Analysis

To investigate the tendency of mean pressure changes in the y direction, three planes parallel to the x-z plane ($y = 1240$ μm, 620 μm, 0 μm) were added to the model shown in Figure 10(a). When the inlet velocity was set as 0.01 mm/s, the mean inlet pressure was 0.412 Pa. Figure 11 indicates that the plane ($y = 1240$ μm) near the inlet has a mean pressure of 0.103 Pa. However, the value decreased rapidly in the y direction, such that it was only 0.011 Pa on the plane near the outlet. In other words, the fluid energy decreased rapidly in the y direction. From the perspective of mass flow, the same conclusion can be drawn. The outlets were named as bottom 1, 2, 3 and side 1, 2, 3 as shown in Figure 10(b). The mass flow in the bottom outlets decreased from the center to the edge, and the mass flow in the side outlets decreased from the top to the bottom, as shown in Figure 12. Moreover, the total mass flow in the side face (1.49×10^{-6} kg/s) was approximately 24.3 times higher than that in the bottom face (6.13×10^{-8} kg/s). From the monitoring record of the flowmeter in the perfusion bioreactor, the total mass flow in the side face (1.35×10^{-6} kg/s) was approximately 22.4 times

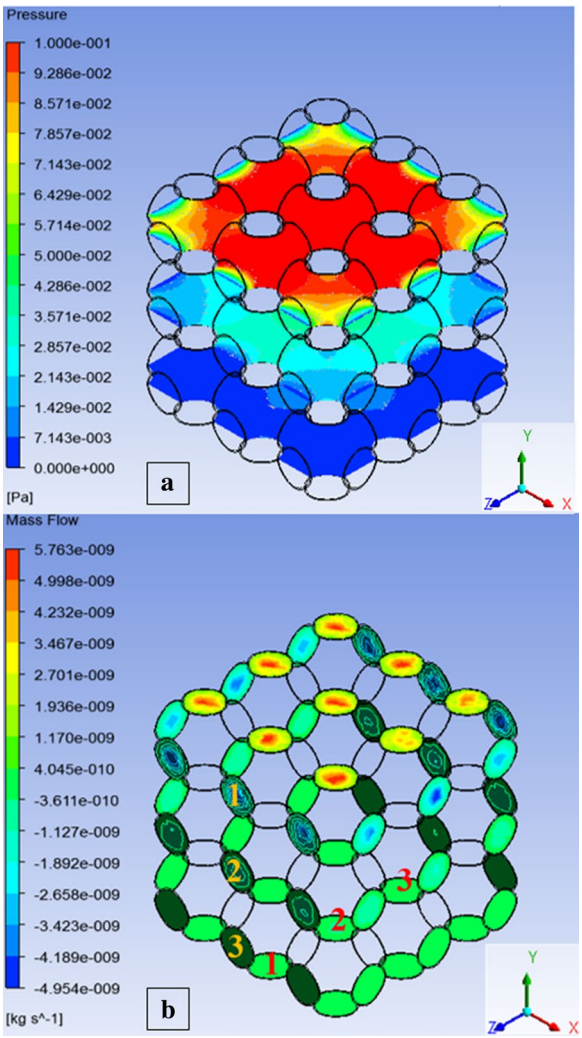

Figure 10 Locations of planes and outlets: **a** three planes, **b** bottom and side outlets

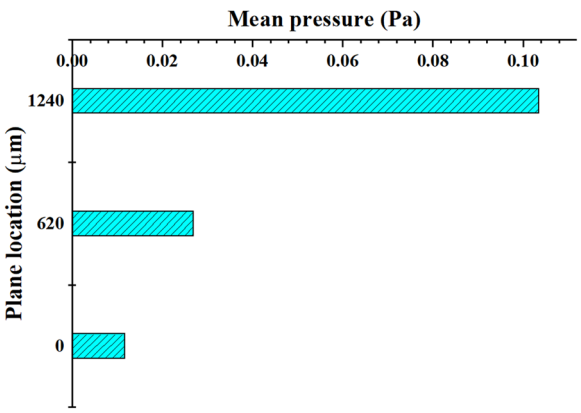

Figure 11 Mean pressure in the three planes obtained using CFD simulation (the pore diameter is 434 μm)

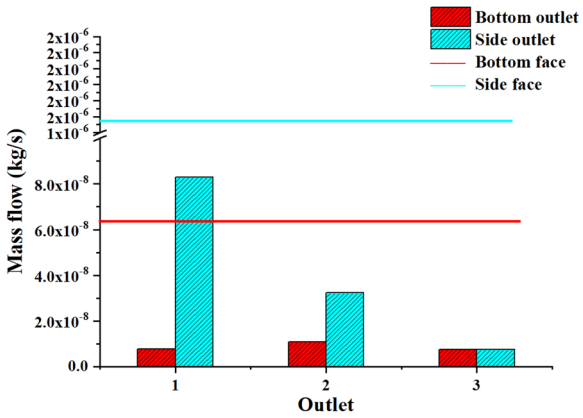

Figure 12 Mass flow in the outlets obtained using CFD simulation (the pore diameter is 434 μm)

higher than that in the bottom face (6.02×10^{-8} kg/s). However, both these values were lower than the corresponding CFD simulation results as shown in Figure 13, because of the shrinkage of the pore diameter and porosity.

As the 27-unit model was periodic in the three directions, a simplified single-unit model is presented in Figure 14 to investigate the flow field performance and to reduce computing time simultaneously.

The inlet velocity of the model was set as 0.0025 m/s, 0.005 m/s, 0.0075 m/s, and 0.01 m/s. The results show that the inlet pressure increases rapidly from 0.052 Pa to 0.394 Pa, i.e., almost eight times, as the velocity increases. According to existing studies, the wall shear stress has a more significant influence on the cell proliferation than the fluid pressure, but the inlet pressure influences the mass flow of the nutrient liquid in a scaffold directly.

When the pore diameter is 314 μm, the mass flow in the bottom outlets increases from 4.821×10^{-8} kg/s to 1.351×10^{-7} kg/s with an increase in the inlet velocity from 0.0025 m/s to 0.01 m/s as illustrated in Figure 15. Furthermore, when the inlet velocity is 0.01 m/s, the mass flow in the bottom outlets increases from 1.351×10^{-7} kg/s to 2.161×10^{-7} kg/s with an increase in the pore diameter from 314 μm to 434 μm. However, the experimentally obtained mass flow value is slightly lower than the CFD simulated value, whereas the variation tendency is the same, as shown in Figure 16 and Figure 17. Several factors contributed to the errors, but the most important factor is the machining error of the scaffolds; another important reason is that the cell culture medium was assumed to be a homogeneous Newtonian fluid.

Figure 18 shows that the mass flow in the side outlets also increases with an increase in the inlet velocity and

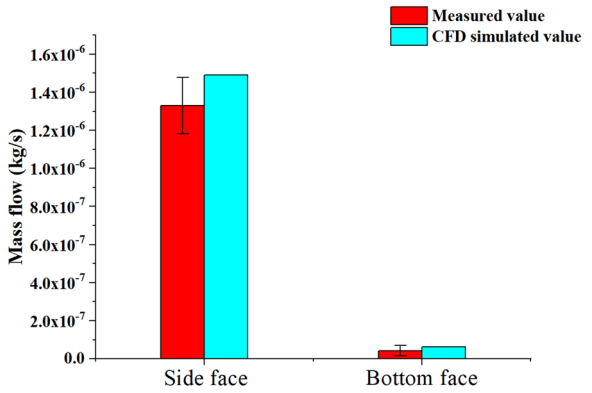

Figure 13 Mass flow in the outlets obtained using CFD simulation and actual measurement (the pore diameter is 434 μm)

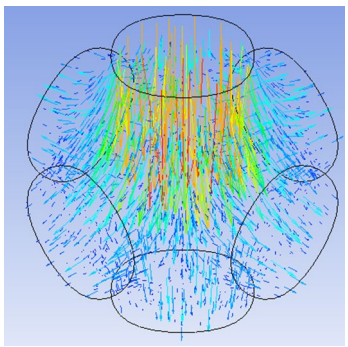

Figure 14 Single-unit model in CFD software

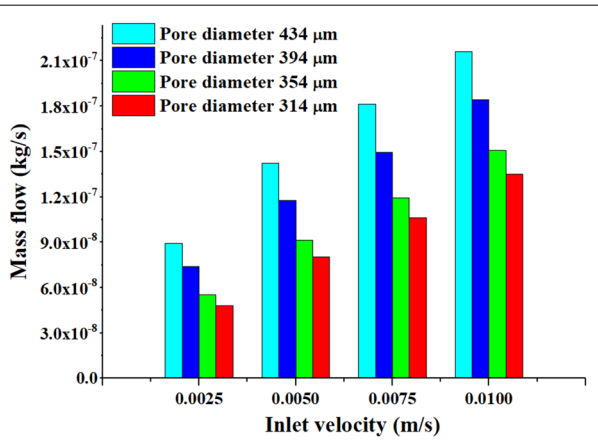

Figure 15 Mass flow in the bottom outlets obtained using CFD simulation

pore diameter. From this perspective, the mass flow in each outlet (bottom or side) was not uniformly distributed. Therefore, in the future studies, our perfusion bioreactor will be improved, and the dynamic cell culture

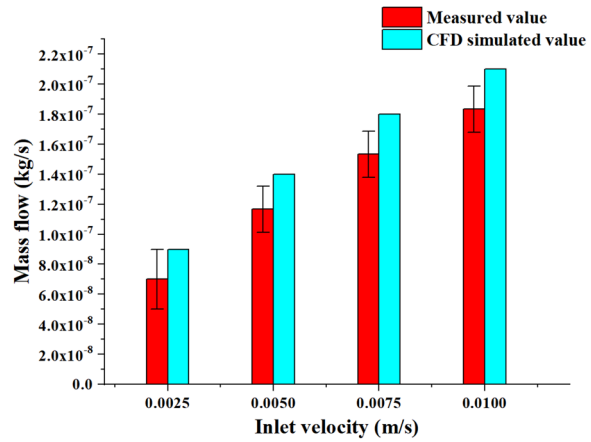

Figure 16 Mass flow in the bottom outlets obtained using CFD simulation and actual measurement (the pore diameter is 434 μm)

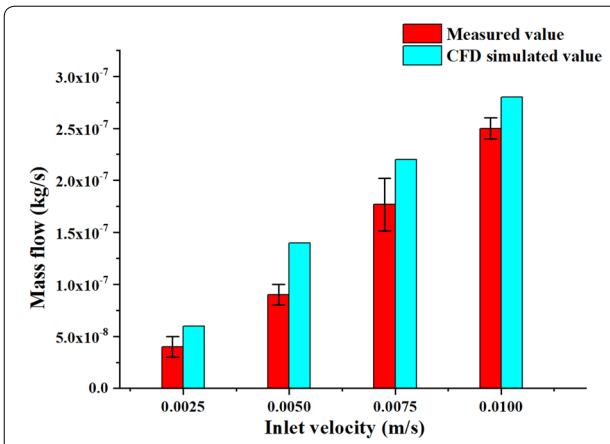

Figure 17 Mass flow in the side outlets obtained using CFD simulation and actual measurement (the pore diameter is 434 μm)

method in 3D environment will be changed to multiple inlets, not only top inlets.

Fluid wall shear stress is an important factor that can influence cell proliferation and differentiation. Porter et al. [26] investigated the velocity and wall shear stress in the scaffold using a lattice Boltzmann method, compared the result with the experimental data, and observed that the most suitable wall shear stress was 5×10^{-5} Pa for osteoclasts, with the upper limit value of 0.057 Pa. Beyond this value, the growth of osteoclasts was severely inhibited.

The velocity field was obtained by solving Navier–Stokes Eq. (3) at every point of the meshing model. Subsequently, the wall shear stress of the Newtonian fluid could be estimated by multiplying the symmetric part of the gradient of the velocity field with the dynamic viscosity of the cell culture medium [26], as described by Eq. (4):

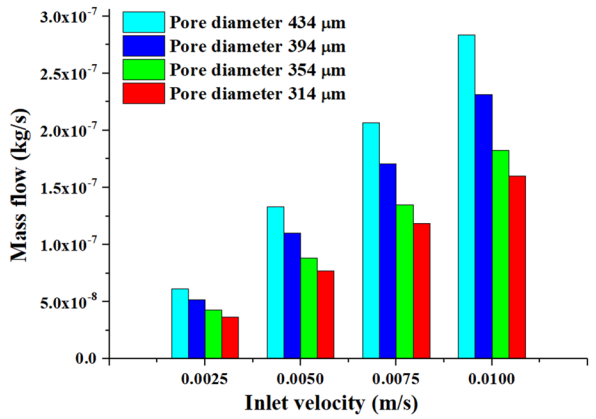

Figure 18 Mass flow in the side outlets obtained using CFD simulation

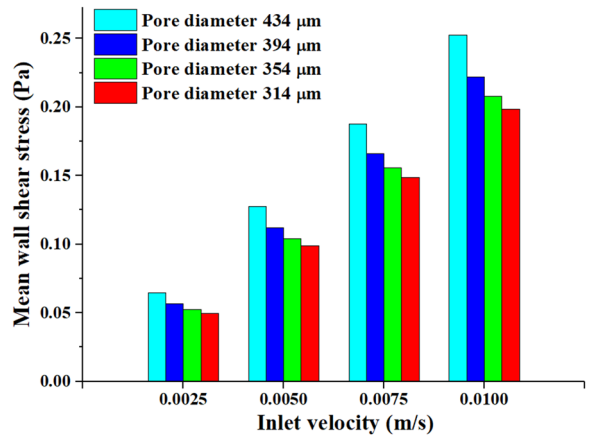

Figure 19 Mean wall shear stress with different pore diameters and inlet velocities

$$\tau = \mu\left(\frac{1}{2}\right)\left(\nabla U + \nabla U^{\mathrm{T}}\right), \tag{4}$$

where τ is the shear stress tensor, μ is the experimental dynamic viscosity, and U is the 3D velocity vector.

Figure 19 illustrates that a larger diameter and faster inlet velocity can yield higher mean wall shear stress. Although all the mean wall shear values were over 0.05 Pa, there was still a large area with a suitable shear stress below 0.05 Pa as shown in Figure 20. A very small area near the inlet had an extremely high value, thus increasing the mean value by a large margin.

3.3 Cell Proliferation Performance

The MTT assay was utilized to determine the cell proliferation performance of the BMSCs on the scaffold samples. The optical density value, read on the UV–vis spectrophotometer after 1, 4, 7, and 10 days, can indirectly reflect the cell proliferation rate as shown in Figure 21. With the progress of time from the 1st day to the 10th day, the BMSCs seeded on the scaffold grew fast, which indicated that the cells were compatible with the designed bone scaffold based on TPMS. Notably, the inlet velocity had a significant impact on the cell proliferation performance. As shown in the results, 0.0075 m/s was the

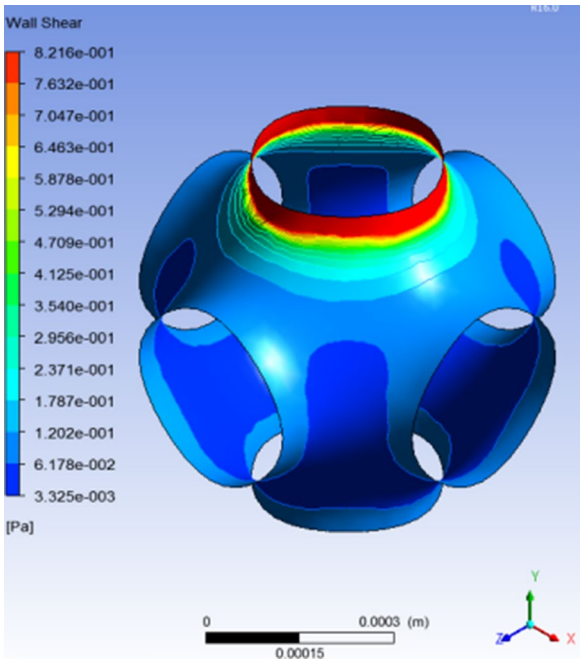

Figure 20 Wall shear stress contour in CFD software

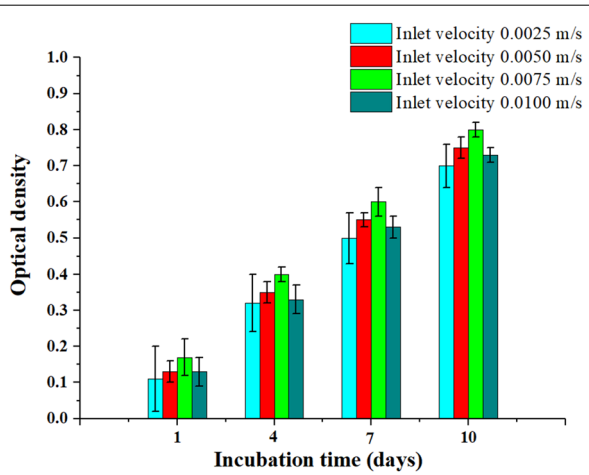

Figure 21 Optical density indicating the cell proliferation performance (the five identical scaffold samples were seeded with BMSCs, and the pore diameter is 434 μm)

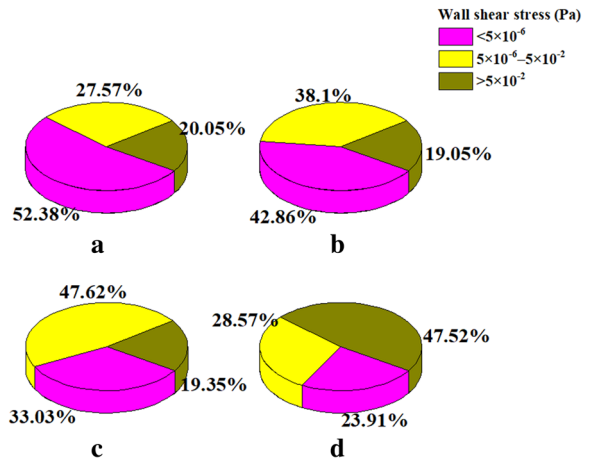

Figure 22 Wall shear stress distribution obtained using CFD simulation (the pore diameter is 434 μm, and the inlet velocity of a, b, c, and d is 0.0025 m/s, 0.005 m/s, 0.0075 m/s, and 0.01 m/s, respectively)

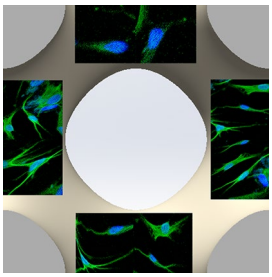

Figure 23 Fluorescence image (assembled with eight images, with the inlet velocity 0.0075 m/s on the 10th day)

most suitable velocity among the four values (0.0025 m/s, 0.005 m/s, 0.0075 m/s, and 0.01 m/s).

Figure 22 shows the proportion of different shear stresses on the scaffold wall calculated using CFD simulation, illustrating that the area with low wall shear stress ($<5\times10^{-6}$ Pa) shrank from 52.38% to 23.81% with the increase in the inlet velocity from 0.0025 m/s to 0.01 m/s. In addition, the area with the high wall shear stress ($>5\times10^{-2}$ Pa) expanded rapidly from 19.35% to 47.62%, with the increase in the inlet velocity from 0.0075 m/s to 0.01 m/s. The area with the suitable wall shear stress (5×10^{-6} Pa–5×10^{-2} Pa) was the largest, when the inlet velocity was 0.0075 m/s, which coincided with the experimental results of the cell proliferation performance as shown in Figure 23.

Both the geometrical shape of the scaffolds and the inlet velocity of the cell culture medium influenced the internal flow field, which in turn had an important effect on the cell proliferation performance in the scaffolds. Figure 23 shows the cell distribution on the scaffold surface on the 10th day, which indicates that most cells grew near the side outlets, whereas only a few cells became attached near the top inlet, corresponding to the wall shear distribution as shown in Figure 20. However, there was an extremely high wall shear stress value (> 0.8 Pa) concentrated near the top inlet, which was not suitable for cell proliferation.

4 Conclusions

(1) A novel method was proposed to design the structure of bone tissue engineering scaffolds based on TPMS. Reverse engineering was utilized to process the point cloud data obtained from an implicit function of TPMS. Solid scaffold models were obtained by using commercial CAD software (SolidWorks) with four different pore diameters 314 μm, 354 μm, 394 μm, and 434 μm, through Thicken and Boolean operations. This method has a high degree of design freedom to obtain scaffold models with different geometric parameters such as pore diameters, porosities, and wall areas.

(2) The fluid field was simulated through a numerical method based on finite volume and the cell proliferation performance was evaluated through an in vitro experiment. The cell distribution on the surface of the TPMS scaffold and the mass flow in the bioreactor verified the flow field simulated using the CFD method. It is concluded from the results that the perfusion inlet should be improved because the mass flow from 4.821×10^{-8} kg/s to 1.351×10^{-7} kg/s was not uniformly distributed in the TPMS scaffold. Moreover, a very high shear stress value up to 0.821 Pa was concentrated on the wall near the inlet of the scaffold. However, there was still a very large area with a suitable shear stress for cell growth, and the inlet velocity 0.0075 m/s was more appropriate than the other three values.

(3) It is feasible to fabricate the TPMS scaffold via 3D printing technology, but the machining precision must be improved through different technologies. Moreover, some new biomaterials with better performance in terms of both mechanical and biological properties should be developed by researchers who are increasingly joining this promising field. Through the analysis of the flow field in the scaffold, this study provides guidance for future studies on the design of bone tissue engineering scaffolds, and on the relationship between cell proliferation and the flow field.

Authors' Contributions
ZW was in charge of the whole trial; ZW wrote the manuscript; CH, JW, PW, SB and CA assisted with sampling and laboratory analyses. All authors read and approved the final manuscript.

Author Details
[1] Centre for Advanced Jet Engineering Technologies (CaJET), Key Laboratory of High-efficiency and Clean Mechanical Manufacture (Ministry of Education), School of Mechanical Engineering, Shandong University, Jinan 250061, China. [2] School of Mechanical and Manufacturing Engineering, The University of New South Wales (UNSW), Sydney, NSW 2052, Australia.

Authors' Information
Zhen Wang, born in 1991, is currently a PhD candidate at *School of Mechanical Engineering*, *Shandong University*, *China*. He received his bachelor degree from *Wuhan University of Technology*, *China*, in 2014. His research interests include additive manufacturing and bio-manufacturing.

Chuanzhen Huang, is currently a professor at *Shandong University*, *China*. He received his PhD degree from *Shandong University of Technology*, *China*. His research interests include ceramic tool materials, precision machining and machining reliability, etc.

Jun Wang, born in 1960, is currently a professor at *University of New South Wales (UNSW)*, *Australia* with a conjoint appointment in *Shandong University*, China and several other universities. He obtained his PhD degree from *University of Melbourne*, *Australia*, in 1993. His main research interest is in advanced manufacturing technologies, in particular, traditional and non-traditional material removal processes.

Peng Wang, born in 1992, is currently a PhD candidate at *School of Mechanical Engineering*, *Shandong University*, *China*.

Shisheng Bi, born in 1991, is currently a master candidate at *School of Mechanical Engineering*, *Shandong University*, *China*.

Ch Asad Abbas, born in 1993, is currently a PhD candidate at *School of Mechanical Engineering*, *Shandong University*, *China*. He received his bachelor degree from *University of Engineering and Technology Taxila*, *Pakistan*. His research area is advanced manufacturing technology.

Competing Interests
The authors declare that they have no competing interests.

Funding
Supported by National Natural Science Foundation of China (Grant Nos. 51675312, 51375273).

Received: 5 September 2017 Accepted: 18 February 2019
Published online: 07 March 2019

References
[1] C Li, D Liu, Z Zhang, et al. Triple point-mutants of hypoxia-inducible factor-1α accelerate in vivo angiogenesis in bone defect regions. *Cell Biochemistry & Biophysics*, 2013, 67(2): 557–566.
[2] C Seebach, D Henrich, K Wilhelm, et al. Endothelial progenitor cells improve directly and indirectly early vascularization of mesenchymal stem cell-driven bone regeneration in a critical bone defect in rats. *Cell Transplantation*, 2012, 21(8): 1667–1677.
[3] R Langer, J P Vacanti. Tissue engineering. *Science*, 1993, 260(5110): 920–926.
[4] U A S And, J P Vacanti. Tissue engineering: current state and prospects. *Annual Review of Medicine*, 2001, 52(1): 443–451.
[5] Y Yan, X Wang, Y Pan, et al. Fabrication of viable tissue-engineered constructs with 3D cell-assembly technique. *Biomaterials*, 2005, 26(29): 5864–5871.
[6] P J Bártolo, M Domingos, T Patrício, et al. Biofabrication strategies for tissue engineering. *Advances on Modeling in Tissue Engineering*, 2011: 137–176.
[7] W U Rendong. Research situation of rapid prototyping techniques used for tissue engineering scaffold. *Journal of Mechanical Engineering*, 2011, 47(5): 170–176.
[8] C Yan, H Liang, A Hussein, et al. Ti–6Al–4V triply periodic minimal surface structures for bone implants fabricated via selective laser melting. *Journal of the Mechanical Behavior of Biomedical Materials*, 2015, 51: 61–73.
[9] S Fujibayashi, M Neo, H M Kim, et al. Osteoinduction of porous bioactive titanium metal. *Biomaterials*, 2004, 25(3): 443–450.
[10] P Heinl, L Müller, C Körner, et al. Cellular Ti-6Al-4V structures with interconnected macro porosity for bone implants fabricated by selective electron beam melting. *Acta Biomaterialia*, 2008, 4(5): 1536–1544.
[11] M Larsson, O Terasaki, K Larsson. A solid state transition in the tetragonal lipid bilayer structure at the lung alveolar surface. *Solid State Sciences*, 2003, 5(1): 109–114.
[12] S T Hyde. Bicontinuous structures in lyotropic liquid crystals and crystalline hyperbolic surfaces. *Current Opinion in Solid State & Materials Science*, 1996, 1(5): 653–662.
[13] S Andersson. On the description of complex inorganic crystal structures. *Angewandte Chemie International Edition in English*, 1983, 22(2): 69–81.
[14] L E Scriven. Equilibrium bicontinuous structure. *Nature*, 1976, 263(5573): 123–125.
[15] F P W Melchels, A M C Barradas, C A V Blitterswijk, et al. Effects of the architecture of tissue engineering scaffolds on cell seeding and culturing. *Acta Biomaterialia*, 2010, 6(11): 4208–4217.
[16] F P Melchels, K Bertoldi, R Gabbrielli, et al. Mathematically defined tissue engineering scaffold architectures prepared by stereolithography. *Biomaterials*, 2010, 31(27): 6909–6916.
[17] J L Lagrange. Miscellanea Taurinensia. *Ostwald's Klassiker*, 1760, 47: 173–195
[18] J B M C Meusnier. *Mem. Mathem. Phys. Acad. Sci. Paris*. 1785, 10: 477–510.
[19] H G V Schnering, R Nesper. Nodal surfaces of Fourier series: Fundamental invariants of structured matter. *Zeitschrift Für Physik B Condensed Matter*, 1991, 83(3): 407–412.
[20] C Zhou, P Xie, Y Chen, et al. Synthesis, sintering and characterization of porous nano-structured CaP bioceramics prepared by a two-step sintering method. *Ceramics International*, 2015, 41(3): 4696–4705.
[21] C Zhou, X Ye, Y Fan, et al. Biomimetic fabrication of a three-level hierarchical calcium phosphate/collagen/hydroxyapatite scaffold for bone tissue engineering. *Biofabrication*, 2014, 6(3): 035013.
[22] S L Xu, D C Li, Z Z Chen, et al. Design and fabrication of plla/cpc hardening scaffold. *Journal of Mechanical Engineering*, 2005, 41(12): 122–125. (in Chinese)
[23] S L Xu, D C Li, Y Z Xie, et al. Study of flow field on in vitro construction of tissue engineering bone by a beta-tricalcium phosphate scaffold. *Progress in Biochemistry & Biophysics*, 2006, 33(9): 895–901.
[24] H A Almeida, P J Bártolo. Design of tissue engineering scaffolds based on hyperbolic surfaces: Structural numerical evaluation. *Medical Engineering & Physics*, 2014. 36(8): 1033–1040.
[25] A C S Dantas, D H Scalabrin, R D Farias, et al. Design of highly porous hydroxyapatite scaffolds by conversion of 3D printed gypsum structures-a comparison study. *Procedia CIRP*, 2016, 49: 55–60.
[26] B Porter, R Zauel, H Stockman, et al. 3-D computational modeling of media flow through scaffolds in a perfusion bioreactor. *Journal of Biomechanics*, 2005, 38(3): 543–549.